

Inverted optical bistability and optical limiting in coherently driven exciton-polaritons

Cite as: APL Photonics 8, 046105 (2023); <https://doi.org/10.1063/5.0136380>

Submitted: 25 November 2022 • Accepted: 14 March 2023 • Published Online: 04 April 2023

 M. Furman, A. Opala,  M. Król, et al.



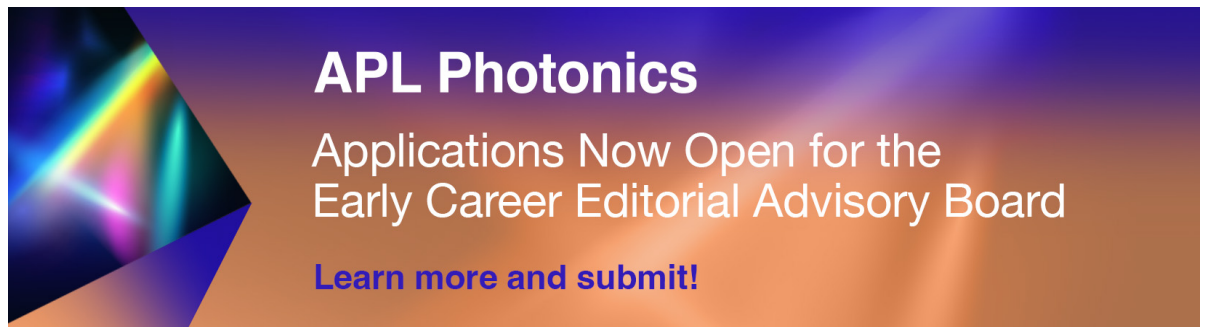
[View Online](#)



[Export Citation](#)



[CrossMark](#)



APL Photonics
Applications Now Open for the
Early Career Editorial Advisory Board
[Learn more and submit!](#)

Inverted optical bistability and optical limiting in coherently driven exciton–polaritons

Cite as: APL Photon. 8, 046105 (2023); doi: 10.1063/5.0136380

Submitted: 25 November 2022 • Accepted: 14 March 2023 •

Published Online: 4 April 2023



M. Furman,¹ A. Opala,^{1,2} M. Król,¹ K. Tyszka,¹ R. Mirek,¹ M. Muszyński,¹ B. Seredyński,¹ W. Pacuski,¹ J. Szczytko,¹ M. Matuszewski,² and B. Piętka^{1,a)}

AFFILIATIONS

¹Institute of Experimental Physics, Faculty of Physics, University of Warsaw, ul. Pasteura 5, PL-02-093 Warsaw, Poland

²Institute of Physics, Polish Academy of Sciences, Aleja Lotników 32/46, PL-02-668 Warsaw, Poland

^{a)}Author to whom correspondence should be addressed: barbara.pietka@fuw.edu.pl

ABSTRACT

Exciton–polaritons in optical cavities exhibit strong nonlinearities predominantly because of the third-order Kerr-like interactions mediated by the excitonic component. Under quasi-resonant excitation, depending on the energy of the incident laser, it results in the optical limiting or bistable behavior. The latter phenomenon is manifested by the hysteresis loop observed in the input–output power characteristics, when a cavity is quasi-resonantly driven by a laser field. The direction of the loop is typically counterclockwise when increasing and subsequently decreasing the optical power. In this work, we demonstrate the optical bistability with an inverted hysteresis direction. It is observed in an exfoliated CdTe-based semiconductor microcavity when the frequency of the pumping laser is tuned slightly below the lower polariton mode. This unusual behavior is caused by the interplay of the suppression of strong coupling and the redshift of the lower polariton mode energy when increasing the incident power. We show that under these conditions, the polariton microcavity can be used as an optical limiter. All of the experimental observations, the shape and the direction of the hysteresis and the optical limiting behavior, are fully supported by a theoretical model.

© 2023 Author(s). All article content, except where otherwise noted, is licensed under a Creative Commons Attribution (CC BY) license (<http://creativecommons.org/licenses/by/4.0/>). <https://doi.org/10.1063/5.0136380>

I. INTRODUCTION

The resonant nonlinear effects are extensively explored in optical microcavities due to their variety and wide range of applications.^{1,2} Two of the most fascinating phenomena include optical bistability and optical limiting.

Bistability is a property of a system that has two stable, stationary states for a certain range of conditions. It is a widely studied phenomenon in nonlinear physics. It can occur in systems that exhibit memory.^{3,4} Bistability manifests itself by the formation of a hysteresis loop when the parameters of the system are adiabatically changed. Concerning optical systems, the bistable behavior arises when a nonlinear medium is incorporated in an optical resonator,⁴ which has been widely studied in different configurations.^{5–7} Apart from that, the optical bistability appears also in diverse systems, e.g., cold atoms,^{8–10} lasers,^{11–13} photonic structures,^{14,15} VCSELs,^{16–18} semiconductor monolayers,¹⁹ metallic gratings,²⁰ and

semiconductor microcavities in the strong coupling regime. In this work, we concentrate solely on the last system. We report on the observation of clockwise hysteresis loop, in contrast to the typical behavior for this kind of structures.

Semiconductor microcavity containing quantum wells (QWs) is an example of an optical resonator with strong nonlinear effects. In the strong light–matter coupling regime, cavity photons mix with excitons, forming quasiparticles called exciton–polaritons (in short, polaritons). Polaritons, despite their photonic origin, strongly interact with each other via Coulomb interactions due to the excitonic component.

The optical bistability in microcavities in the strongly coupled regime can result from the bleaching of light–matter coupling, as theoretically predicted.²¹ On the other hand, bistability more frequently results from the Kerr-type nonlinearity due to polariton–polariton interactions.^{1,2,22–24} It can be realized under various experimental conditions, typically with quasi-resonant

pumping.^{22,23,25} Moreover, taking into account the polariton spin degree of freedom and polarization of incident light, a multistable behavior has been observed.^{26,27} Additionally, the bi- or multistability of the polariton condensate can also be observed for the non-resonant excitation of the system.^{28–30}

Bistability has been widely studied because of the possible applications of this effect in optical logic circuits,^{31,32} Ising-model simulators,^{33,34} optical switches,^{35,36} or the construction of optical transistors.^{36,37} The spin multistability of polaritons can be used to construct a complete architecture of photonic logic gates.³⁸

In the majority of experiments performed in microcavities based on III–V semiconductors,^{22,39} bistability appears in the form of a hysteresis loop, when the structure is pumped by a laser with energy detuned slightly above the lower polariton mode. In such a configuration, the polariton energy blueshifts with an increase in the pump power and the system switches to a higher transmission state when the polariton energy becomes locked to the laser energy. With a subsequent reduction in the incident power, the system remains locked in the higher transmission state for a certain range of power before switching to the lower transmission state. This range of bistability corresponds to a hysteresis loop in the input–output characteristics. According to the description above, it results in a counterclockwise dependence in the diagram of the output power as a function of the input power.

In this work, we describe the inverted type of bistability that we created in a CdTe-based microcavity. To show the novelty of our results, it is useful to compare the experimental input–output power characteristics measured at two different laser energies. Figure 1(a) illustrates the dispersion relation of polariton modes, with quasi-resonant laser energies marked with (1) and (2). When the energy of the laser is above the lower polariton mode energy, as in the case of (1), the measured input–output power characteristics are presented in Fig. 1(b). It exhibits a counterclockwise direction and

qualitatively resembles the hysteresis loop reported previously in the literature.^{22,39} However, when the laser energy is below the lower polariton energy, as in the case of (2), the system develops another hysteresis loop, which exhibits an unexpected shape. This new type of optical bistability with an inverted (clockwise) hysteresis direction is shown in Fig. 1(c). As the input power is increased, the transmitted light intensity increases linearly. Furthermore, the system abruptly switches from the strong coupling regime to the weak coupling regime, which is observed as a sudden drop in the transmitted light intensity. As the excitation power is then reduced, the system remains in the weakly coupled state for a certain range of input power. This leads to the formation of a hysteresis loop with a clockwise direction, opposite to the optical bistability observed due to the Kerr-like nonlinearity.

Moreover, from the point of view of applications, the measured input–output characteristics exhibit a behavior that is essential for the so-called optical limiters.^{40–42} Optical limiting is an effect where the transmitted light intensity does not increase above a certain threshold pumping power. Optical limiters are useful elements in photonic systems that allow low light intensities to pass but simultaneously protect sensitive elements by blocking high laser intensities. Various physical effects can be used in optical limiters: multi-photon absorption,^{43–45} reverse saturated absorption,^{46,47} self-defocusing,⁴⁸ or nonlinear scattering.^{49,50} Optical limiting can be realized in a wide range of structures, such as photonic crystals,⁵¹ micro-ring resonators,⁵² waveguides,^{53,54} microcavities,^{43,55} or microcavities in the strong coupling regime.^{2,56}

This work is organized as follows: Sec. II describes the preparation of the sample, with an emphasis on the exfoliation process of a CdTe-based microcavity from a GaAs substrate. The experimental results are presented in Sec. III. These consist of the results from quasi-resonant transmission intensity studies at different energies of the incident laser and the angle-resolved luminescence as a function of excitation power. We theoretically explain all the effects in terms of suppression of strong coupling and polariton energy reduction and compare them with the case of Kerr-type interactions in Sec. IV.

II. PREPARATION OF THE SAMPLE

We studied a CdTe-based semiconductor microcavity in a transmission configuration. The growth of such microcavities has been carried out in two types of substrates: CdTe^{57–59} and GaAs,⁶⁰ but both are nontransparent in the spectral region of excitons in CdTe QWs. For this reason, the substrate (in our case, GaAs) has to be removed after growth.

Typically, during the preparation of the semiconductor microcavity samples for transmission measurements, the substrate is mechanically thinned and polished.⁶¹ Another approach is chemical etching, which has been performed on microcavities⁶² and on other layered devices.⁶³

Within this work, the sample was prepared using a novel approach based on the lift-off method utilizing a sacrificial buffer layer.⁶⁴ The additional sacrificial layer, grown between the microcavity structure and the GaAs substrate, allows for the water exfoliation process to remove the nontransparent substrate and create a transmissive structure.⁶⁵ The microcavities prepared in this way retain a high optical quality, as evidenced by the observation of the strong

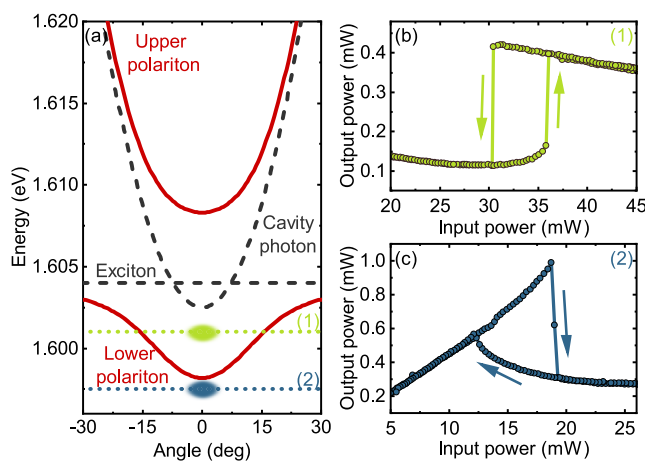


FIG. 1. Types of bistability observed in the system. (a) Dispersion relation of polariton modes (red lines) resulting from the strong coupling between the cavity photon and quantum well exciton (dashed black lines). The colored dotted lines mark two different laser energies (1) and (2). (b) Optical input–output characteristics with a counterclockwise hysteresis loop measured at laser energy (1). (c) Optical input–output characteristics with a clockwise triangular hysteresis loop measured at laser energy (2).

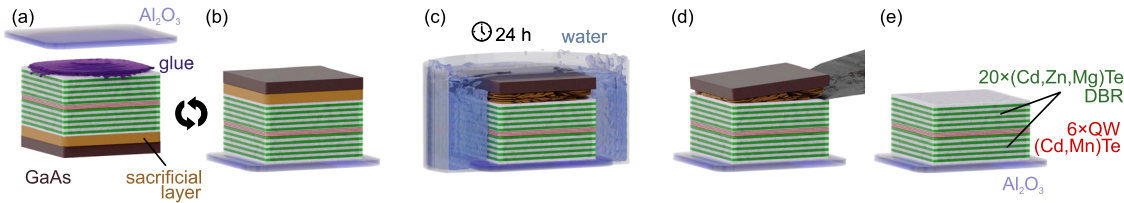


FIG. 2. Process of creating a transmissive microcavity based on CdTe. (a) The transparent Al_2O_3 substrate sticking to the cavity, (b) the cavity with the new substrate attached, (c) the cavity immersed in deionized water for about 24 h, (d) piling off the nontransparent substrate, and (e) the exfoliated cavity on the transparent substrate.

coupling regime and polariton condensation (see the [supplementary material](#)).

In the investigated sample, a 90 nm MgTe sacrificial buffer layer was grown between the substrate and the microcavity structure. The water exfoliation method used to dissolve the hygroscopic MgTe layer and for detaching the cavity from the substrate utilized in this work is schematically presented in [Fig. 2](#). At first, the semiconductor structure was glued to a transparent sapphire (Al_2O_3) surface. The size of the sapphire was larger than the microcavity. A drop of glue was placed on the sample. Then, the sapphire surface was placed on it so that the nontransparent GaAs substrate was on top, as shown in [Fig. 2\(a\)](#). The stack was pressed against the sapphire. The excess glue flowing to the sides was removed with a toothpick to allow water to reach the MgTe layers in order to degrade the sacrificial layer [[Fig. 2\(b\)](#)]. The structure was then placed in a beaker with water and left for 24 h [[Fig. 2\(c\)](#)]. After that, the sample was dried with nitrogen gas and left under ambient conditions for another 24 h. Next, the nontransparent GaAs was detached, as shown in [Fig. 2\(d\)](#), leaving the microcavity structure glued to the sapphire, as presented in [Fig. 2\(e\)](#). Thanks to the use of the lift-off method, a CdTe-based microcavity, grown on the nontransparent GaAs, was finally secured on a transparent sapphire substrate.

In detail, the investigated semiconductor optical microcavity structure consisted of two Bragg mirrors (DBRs), each made of 20 pairs of alternating CdTe layers alloyed with magnesium and zinc. The 600 nm thick cavity between the DBRs was formed by a (Cd,Zn,Mg)Te layer. Within the cavity layer, 6 CdTe:Mn QWs were placed at the maxima of the electric field distribution.

III. EXPERIMENTAL RESULTS

The transmissive semiconductor microcavity obtained by the wet exfoliation process was located in a cryostat at a temperature of 4.5 K.

Measurements were performed to determine the dependence of the intensity of the light transmitted through the sample on the power of the incident laser beam. Such input–output optical power characteristics were collected at various energies of the laser, tuned in the spectral region of the lower polariton mode. A linearly polarized continuous wave laser beam from a tunable Ti:sapphire source was focused on the sample using a lens with a focal length $f = 25.4$ mm. The diameter of the laser spot on the sample was around $12\ \mu\text{m}$. The transmitted signal was collected with a $50\times$ microscope objective with a numerical aperture of $\text{NA} = 0.55$. The incident and transmitted laser powers were simultaneously measured by two detectors: one placed before the cryostat and the second one behind

the sample. The laser power was changed in the range from single microwatts to tens of milliwatts. The incident power was automatically adjusted in a continuous manner with the angle of a half-wave plate mounted on a programmable rotation stage before a linear polarizer.

The input–output power characteristics, measured for different laser energies, are shown in [Fig. 3](#). Detuning is defined as the energy difference between the laser energy and the minimum of the lower polariton branch, $\delta = E_P - E_{LP}(\mathbf{k} = 0)$. In the case of laser energy (1), at $\delta = 4.1$ meV, a hysteresis loop was observed in the 30–40 mW input power range. While increasing the power of the incident laser, the system abruptly switched to a higher transmission state at around 38 mW. While reducing the incident optical power, the system switched to a lower transmission state at around 33 mW, forming a hysteresis loop with a counterclockwise direction. Although the observed input–output characteristics resemble the optical bistability originating from the Kerr-like nonlinearity of lower polaritons, in our system, it has a different origin. As will be discussed in detail in [Sec. IV C](#), here, it is a result of the energy crossing between the laser and the strongly redshifting upper

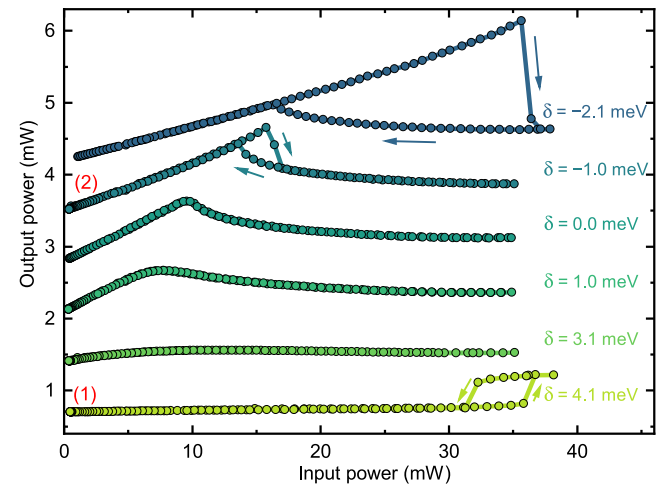


FIG. 3. Dependence of the optical power transmitted through the sample on the input power measured for various energies of the incident laser. The lines numbered (1) and (2) show the input–output characteristics of two different types of optical bistability for laser energies corresponding to [Figs. 1\(b\)](#) and [1\(c\)](#). The plots are spaced out in the vertical direction so that the first dependence in the figure is in the original scale. The lines are labeled with the detuning between the laser energy and the lower polariton mode minimum δ .

polariton mode. As the laser energy is detuned closer to the lower polariton, this hysteresis loop shifts toward higher pumping powers.

As the energy was decreased to approach the minimum of the lower polariton branch, the bistable behavior for the input power around 30 mW moved away from the measured range of pumping powers. Under these conditions, the system acts as an optical limiter. For laser detuning $\delta = 1.0$ meV above the lower polariton mode, the transmitted light intensity increases almost linearly with the input power up to 7.5 mW. Then, the optical limiting occurs, with the transmitted power being almost independent of the excitation intensity. At $\delta = 0$ meV, the range of linear input–output dependence increases to 10 mW. For higher pump intensities, the output power slightly decreases and saturates.

When the laser energy is tuned below the minimum of the lower polariton mode, a qualitatively different phenomenon emerges. We observe a new hysteresis loop with the direction inverted with respect to the common counterclockwise hysteresis. It has a triangular shape and stems from a cusp formed at the maximum of transmitted power. The appearance of a new type of hysteresis is the result of physical processes that will be discussed in detail alongside our theoretical model in Sec. IV. As the pumping power was increased, for $\delta = -1.0$ meV, the transmitted laser power increased linearly up to 15.8 mW, when it abruptly switched to a lower transmission state. The switching is related to the transition of the system from the strong coupling to the weak coupling regime (Sec. IV C). With a further increase in the incident laser power, the transmitted light intensity slowly decreased. However, when the incident laser power was decreased, the system remained in a lower transmission state until 13.6 mW, completing the clockwise hysteresis loop. As the energy of the incident laser was tuned further down below the lower polariton mode [$\delta = -2.1$ meV, (2)], the bistability range broadened and shifted to higher input powers.

To better understand the observed phenomenon, the laser energy was adjusted to the minimum energy of the lower polariton mode, which corresponds to the appearance of the inverted hysteresis. The measured input–output characteristics in Fig. 4(a) show the switching between the strong and weak coupling at 18 mW, accompanied by a sudden drop in the transmitted light intensity. The experimental setup was then modified to allow for angle-resolved measurements by Fourier space imaging of the light emitted from the microcavity (for details, see the [supplementary material](#)). The weak luminescence from the microcavity was directed to the slit of the spectrometer, and the high intensity of transmitted laser light was cut out with a bandpass filter.

The acquired polariton dispersion relations at different excitation powers are presented in Figs. 4(b)–4(d). In Fig. 4(b), which shows the dispersion relation for 6.79 mW input power, two modes of upper and lower polaritons are clearly visible. A Rabi splitting of 7 meV was obtained from the coupled oscillator model [see Eq. (A.1) in the [Appendix](#)] fitted to the measured angle-resolved spectra. The corresponding modes of the upper and lower polaritons are marked with the red lines, while the corresponding bare cavity photon and exciton energies are depicted with the black dashed lines. Similarly, in Fig. 4(c), which corresponds to the power just before the transition to the lower transmission state, both polariton modes can be seen. The coupling strength decreased to 3 meV, but the system remains in the strong coupling regime. In Fig. 4(d), for a

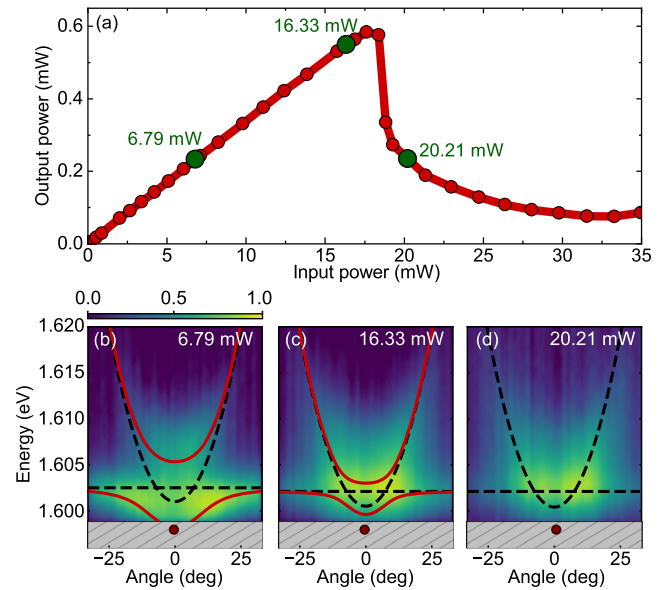


FIG. 4. (a) Input–output power characteristics collected for the laser energy tuned to the minimum of the lower polariton mode ($\delta = 0$). The green dots mark the input power values for which luminescence dispersions with an angular resolution were measured. (b)–(d) Normalized luminescence spectral maps obtained from the cavity transmission for three different pumping powers. Polariton modes as well as photon and exciton modes were fitted in the maps (red lines). This allowed us to show how the coupling strength in the system changes with pumping power. Spectra (b)–(c) correspond to the strong coupling regime, while dispersion relation (d) shows the situation after the system went into the weak coupling regime. The hatched region in (b)–(d) marks the spectral region covered up by the bandpass filter.

power just above the transition (20.21 mW), only a single mode with a parabolic dispersion is visible. The system transitioned from the strong to weak coupling regime as the light–matter coupling strength decreased below the linewidth of polariton modes.

To summarize the experimental results, the investigated exfoliated optical microcavity based on CdTe demonstrated a new type of optical bistability, where the energy of the incident laser was set below the minimum energy of the lower polariton mode. The intensity of the transmitted light formed a hysteresis loop with a clockwise direction. A decrease in the Rabi splitting in the cavity was observed when increasing the pumping power. The switching between the two bistable states was accompanied by the transition between the strong and weak coupling regimes. In addition, as for high excitation powers, the transmitted power decreased, the system can find application as an optical limiter.

IV. THEORY

In order to explain the formation of the inverted hysteresis, the quasi-resonant excitation of an optical semiconductor microcavity was also investigated theoretically. At first, a two-component model is used to obtain the optical input–output characteristics when the system is driven in the spectral vicinity of lower and upper polariton modes. Next, following the experimental observations, we include in the theoretical model the effects of suppression of the coupling

strength⁶⁶ and additionally assume an energy redshift of polariton components.^{67,68} Furthermore, we point out the differences between the inverted hysteresis and the nonlinear optical response of a microcavity with interactions mediated by excitons only. It should be noted that the standard two-component model is insufficient to describe the inverted hysteresis.

A. Two-component model

The evolution of photonic $\psi_C(t)$ and excitonic $\psi_X(t)$ components of polaritons was determined using coupled mean-field equations,^{69,70}

$$i\hbar \frac{d}{dt} \psi_C = (E_C(\mathbf{k}) - i\hbar\gamma_C) \psi_C + \frac{\hbar\Omega_R}{2} \psi_X + F e^{-i\omega_p t}, \quad (1)$$

$$i\hbar \frac{d}{dt} \psi_X = (E_X(\mathbf{k}) - i\hbar\gamma_X + g_X |\psi_X|^2) \psi_X + \frac{\hbar\Omega_R}{2} \psi_C, \quad (2)$$

where $E_{C,X}(\mathbf{k}) = E_{C,X}^0 + \frac{\hbar^2 \mathbf{k}^2}{2m_{C,X}^*}$ are the dispersion relations of cavity photons and quantum well excitons (indices C and X, respectively). The parameters $\gamma_{C,X}$ are the loss coefficients of the two components. The Rabi frequency that defines the coupling strength between excitons and photons is given by Ω_R . The last term in the first equation describes the external laser pumping with energy $E_P = \hbar\omega_P$ and amplitude F . The parameter g_X represents the strength of the third-order (Kerr-like) nonlinearity due to the interactions between excitons, which has been crucial in the description of bistability.²²

The model has already been used to explore Rabi oscillations,^{71–74} optical parametric scattering,^{75,76} multistability,^{77,78} and dynamic modification of light–matter coupling,^{66,79} due to the presence of two degrees of freedom. In this work, it is used to simulate the intensity of the transmitted light for varying intensity and energy of the driving field.

B. Hysteresis near lower and upper polariton branches

We begin our analysis with the standard model of bistability where the loss of strong coupling is neglected and the exciton–exciton interactions are the only source of nonlinearity. The calculated optical field density in a microcavity for two different laser energies obtained using Eqs. (1) and (2) is shown in Fig. 5. The simulated density of the photonic field in the steady-state $|\psi_C^{SS}|^2$ is proportional to the intensity of the transmitted light. The amplitude of the pumping field F was continuously varied upward from zero to the maximum value and then back to zero. In Fig. 5(a), the detuning between the laser energy and the energy of lower polariton mode was set to $\delta = 2.09$ meV, for $E_P = -4.25$ meV ($E_P \approx E_{LP}$), which resulted in an “S-shaped” hysteresis between the photonic component density and the external optical input. This input–output counterclockwise hysteresis is expected for lower polaritons and has been widely studied theoretically and experimentally.^{1,2,22}

Although the calculated hysteresis may seem to match the experimental results for laser energy (1) in Fig. 1(b), we encounter qualitative differences for other values of laser detuning. In simulations for excitation with energy $E_P = 6$ meV ($E_P \approx E_{UP}$), slightly above the resonance with the upper dispersion branch, when $\delta = 12.34$ meV, another hysteresis loop with a “triangular” shape,

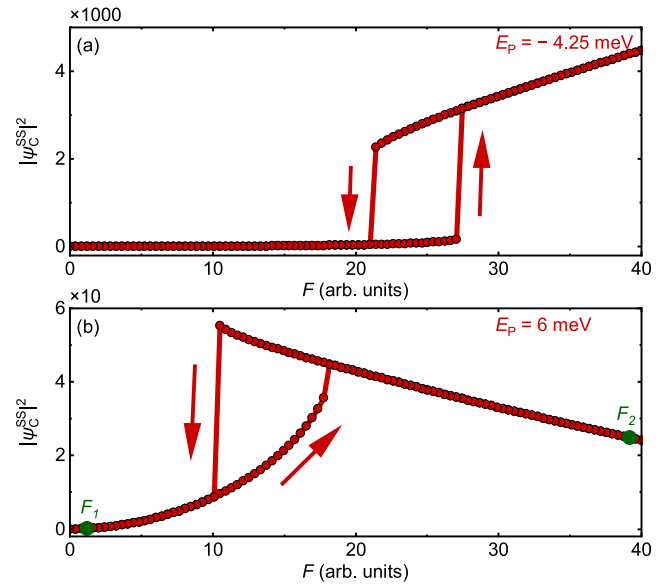


FIG. 5. Hysteresis in the model without the loss of strong coupling for the pump energy near the lower (a) and the upper (b) polariton branches at $\mathbf{k} = 0$. The red dots show the density of the photonic component in steady states for increasing and decreasing laser field amplitude $|F|$. The arrows indicate the direction of the hysteresis. In both cases, the system remains in the lower branch of the hysteresis loop when the laser field intensity is adiabatically increased. The simulation parameters are $\hbar\Omega_R = 10.5$ meV, $E_X = 0$ meV, $E_C = -2$ meV, $\gamma_C = 0.5$ ps⁻¹, $\gamma_X = 0.5$ ps⁻¹, $g_X = 0.02$ meV μm^2 , $E_{UP} = 4.34$ meV, and $E_{LP} = -6.34$ meV.

as shown in Fig. 5(b), is encountered. This nontrivial dependence of the polariton response can be explained by the influence of the Kerr-like nonlinearity on the energy spectrum. The Kerr nonlinearity results in a blueshift of the polariton mode energy with increasing input power.

This effect is analyzed by calculating the response of polaritons to a coherent laser field with a fixed intensity and varying energy (see the Appendix). The calculated energy spectra obtained for two laser amplitudes F_1 and F_2 are shown in Figs. 6(a) and 6(b). Figure 6(a) presents the polariton dispersion when the system is excited with a laser field with energy $E_P = 6$ meV and a low amplitude F_1 . In this case, the energy blueshift $\Delta_B = g_R |\psi_X^{SS}|^2$ is negligibly small and the difference between the exciton and photon energies at $\mathbf{k} = 0$ is equal to 2 meV. The solid lines in Figs. 6(a) and 6(b) indicate the analytically calculated dispersion of the lower and upper polariton branches when $E_X = E_X^0 + \Delta_B$ (see the Appendix). Figure 6(b) presents the energy spectrum of the system excited with the same energy as in (a) but with a higher laser field amplitude F_2 ($F_1 < F_2$). In this case, the energy blueshift induced by the interactions significantly modifies the polariton energy.

The triangular shape of the hysteresis in Fig. 5(b) can be understood as an effect of the modification of the polariton composition. Figure 6(c) shows the photonic (C_U) and excitonic (X_U) Hopfield coefficients for the upper polariton branch.⁸⁰ The upper polaritons become more excitonic for small wave vectors as the optical pump intensity is increased. The calculated difference between the excitonic Hopfield coefficients for upper polaritons at $\mathbf{k} = 0$ for pump

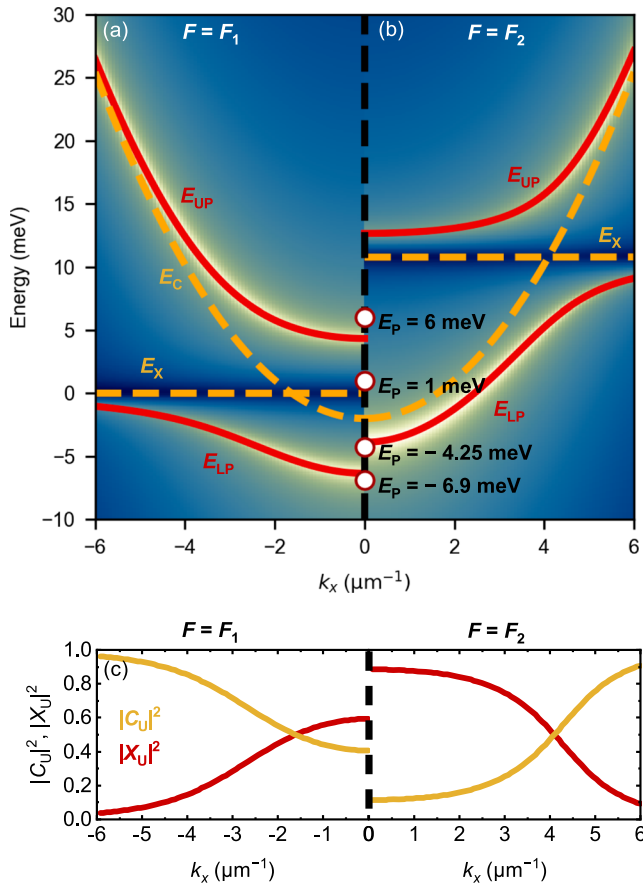


FIG. 6. (a) and (b) Simulated spectrum of a polariton system excited with laser at energy $E_p = 6$ meV and amplitudes F_1 and F_2 marked in Fig. 5(b). We assume that the exciton effective mass and the cavity photon effective mass are $m_C^* = 5 \cdot 10^{-5} m_e^0$ and $m_X^* = 5 \cdot 10^{-1} m_e^0$, respectively, where m_e^0 is the free electron mass. (c) Hopfield coefficients of the upper polariton excited with an optical pump with amplitudes F_1 (left) and F_2 (right).

powers F_2 and F_1 was ~ 0.26 , which explains why the density of the photonic field decreases when increasing the pump power. For laser energy close to the lower polariton mode, an opposite mechanism explains the increase in the photonic component density [Fig. 5(a)].

We note that, in contrast to the experimental observation, the directions of both hysteresis loops in Figs. 5(a) and 5(b) are counterclockwise. To reproduce the experimental clockwise (inverted) hysteresis direction, the model has to be extended to include the effects of the loss of strong coupling and the thermal energy redshift.

C. Inverted hysteresis

To reproduce the experimental observations, we modified the set of equations in the following form:

$$i\hbar \frac{d}{dt} \psi_C = (\tilde{E}_C - i\hbar\gamma_C) \psi_C + \frac{\hbar\tilde{\Omega}}{2} \psi_X + F e^{-i\omega_p t}, \quad (3)$$

$$i\hbar \frac{d}{dt} \psi_X = (\tilde{E}_X - i\hbar\gamma_X + g_X |\psi_X|^2) \psi_X + \frac{\hbar\tilde{\Omega}}{2} \psi_C. \quad (4)$$

The newly introduced $\tilde{E}_{C,X}$ terms reflect the effect of the energy redshift of the photon and exciton components, induced by the thermal effects.^{67,68} The assumption of the energy redshift was required to successfully describe the inverted hysteresis loops. It was assumed that the heating of the sample changes energies quadratically as a function of the pump amplitude, or equivalently, linearly as a function of light intensity. The resulting effective energy of the photon and exciton is given by

$$\tilde{E}_{C,X} = E_{C,X} - \beta_{C,X} |F|^2, \quad (5)$$

where $\beta_{C,X}$ is a phenomenological constant describing the strength of the thermal effects. Phenomenologically, we observe that both exciton and photon modes are redshifted by approximately the same amount for a given pump power ($\beta_C \approx \beta_X$). It should be noted that the thermal energy shifts for the photonic and excitonic modes usually differ in semiconductors. This effect is strongly dependent on the material properties of the system.⁶⁷

The model can also take into account that the density of excitons is locally increased for high-power excitations. In the critical case, the distance between excitons can be comparable to their Bohr radii. At this point, the Pauli exclusion results in the phase space filling effect, which leads to the reduction in the light-matter coupling.⁶⁹ Therefore, the effective Rabi frequency $\tilde{\Omega}$ can be written as

$$\tilde{\Omega} = \Omega_R^0 e^{-(\beta_1 n_R + \beta_2 |\psi_X|^2)}, \quad (6)$$

where $|\psi_X|^2$ and $n_R \approx \alpha \frac{|F|^2}{\gamma_X}$ are the coherent exciton density and the density of incoherent, thermally excited carriers, α is the scaling parameter (for more details, see the [supplementary material](#)), and Ω_R^0 is the value of the Rabi splitting in the case when saturation effects are negligible. The parameters β_1 and β_2 describe how the density of coherent and incoherent carriers affects the reduction in the light-matter coupling.

The response of the polariton system obtained using Eqs. (3) and (4) is shown in Fig. 7. In the simulation, it was assumed that the loss of strong coupling is the most prominent nonlinear phenomenon in the system (compared to the effect of nonlinear exciton-exciton interactions). This assumption is fulfilled when $g_X \ll \beta_2 \Omega_R$. Figure 7(a) shows the hysteresis arising when the system is excited by a laser source with energy close to the upper polariton mode with $\delta = 7.34$ meV ($E_p = 1$ meV). The calculated hysteresis loop has the same direction as in the experimental results obtained for laser energy close to the upper polariton. The measured input-output characteristics in Fig. 1(b) have the same direction and the overall shape of the hysteresis loop.

Within the same model, Fig. 7(b) shows the response of the photonic component that arises when the laser energy was set below the lower polariton branch when $E_p = -6.9$ meV and $\delta = -0.55$ meV. In this case, the hysteresis shape was triangular and was characterized by the rapid depletion of the photon field density at a critical value of the pump power. The direction of the hysteresis was opposite compared to the examples shown in Fig. 5. The hysteresis arising near the lower polariton resulted from the competition between the

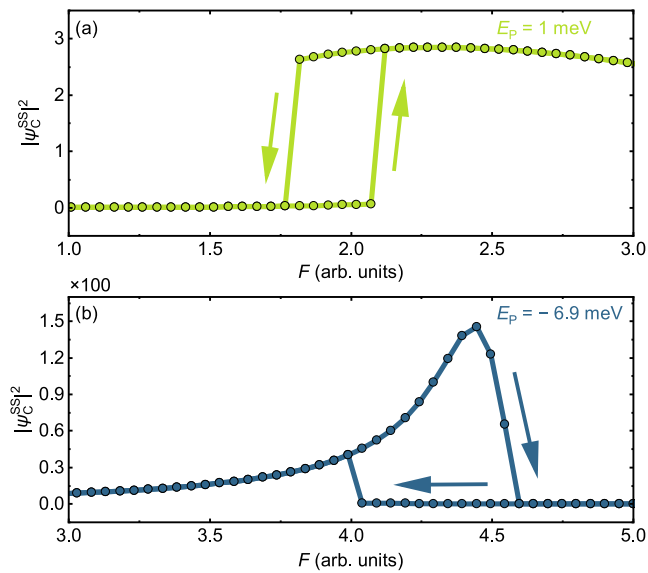


FIG. 7. Hysteresis loops in the model with the loss of strong coupling and thermal energy redshift. The counterclockwise upper polariton (a) and clockwise lower polariton (b) hysteresis for $E_p = 1$ meV and $E_p = -6.9$ meV, respectively. The arrows indicate the direction of the hysteresis. The simulation parameters are $\hbar\Omega_R = 10.5$ meV, $E_X = 0$ meV, $E_C = -2$ meV, $\gamma_C = 0.5$ ps $^{-1}$, $\gamma_X = 0.5$ ps $^{-1}$, $g_X = 0.02$ meV μm^2 , $\mathbf{k} = 0$ μm^{-1} , $\beta = 0.24$, $\beta_1 = 0.001$, $\beta_2 = 0.165$, $\alpha = 1$, $E_{UP} = 4.34$ meV, and $E_{LP} = -6.34$ meV.

loss of strong coupling, exciton–exciton interactions, and thermal energy redshift of excitons and cavity photons. The simulated behavior was once again in good agreement with the experimental results. The initial increase in the transmitted light intensity with a sudden decrease in the transmittance and the resulting clockwise hysteresis loop are observed in Fig. 1(c).

V. SUMMARY

To summarize, the quasi-resonant laser transmission was investigated in an exfoliated II–VI semiconductor microcavity. With increasing laser power, the polariton modes exhibited suppression of the exciton–photon coupling strength, as evidenced by the angle-resolved measurements. For varying excitation power, the transmitted light intensity showed a bistable behavior with hysteresis loops. For the incident laser energy above the lower polariton mode, the hysteresis loop resembled the behavior reported in GaAs-based structures, where it originates from the lower polariton energy blueshift due to Kerr-like nonlinearities. Here, the bistability arose from the energy redshift of the upper polariton mode. Most importantly, when the laser energy was set below the lower polariton mode, the system exhibited a different kind of bistable behavior, showing a hysteresis loop with the opposite direction. As a function of increasing pumping power, the transmittance decreased sharply. We suggest that this transmittance blocking phenomenon can be used in an efficient optical limiter.

All the observed properties were taken into account in the theoretical analysis. Starting from the two-component model with the Kerr-like nonlinear term, the well-known hysteresis loop was

observed for the system driven with a laser tuned at the energy above the lower polariton mode. However, contrary to the experimental results, hysteresis loops due to both upper and lower polaritons exhibited the same (counterclockwise) direction.

To explain the experimental results, the model was extended to take into account the polariton energy redshift and Rabi energy reduction. The simulated input–output characteristics changed significantly. Depending on the energy of the driving field, the hysteresis loops exhibited clockwise or counterclockwise directions, in full agreement with the experimental observations.

SUPPLEMENTARY MATERIAL

See the [supplementary material](#) for additional details of the experimental setup, determination of microcavity quality factor, polariton condensation, and reservoir density in simulations.

ACKNOWLEDGMENTS

This work was supported by National Science Centre, Poland—M.F., M. Ma., and B.P. received funding under Grant No. 2020/37/B/ST3/01657, R.M. received funding under Grant No. 2019/33/N/ST3/02019, and A.O. received funding under Grant No. 2019/35/N/ST3/01379.

AUTHOR DECLARATIONS

Conflict of Interest

The authors have no conflicts to disclose.

Author Contributions

M. Furman: Formal analysis (equal); Investigation (equal); Visualization (equal); Writing – original draft (equal). **A. Opala:** Formal analysis (supporting); Methodology (lead); Writing – original draft (equal). **M. Król:** Investigation (supporting); Writing – original draft (equal). **K. Tyszka:** Investigation (supporting). **R. Mirek:** Investigation (supporting). **M. Muszyński:** Investigation (supporting); Visualization (supporting). **B. Seredyński:** Resources (supporting). **W. Pacuski:** Resources (lead). **J. Szczytko:** Supervision (supporting). **M. Matuszewski:** Methodology (supporting); Supervision (supporting); Writing – review & editing (equal). **B. Piętko:** Funding acquisition (equal); Methodology (equal); Supervision (equal); Writing – review & editing (equal).

DATA AVAILABILITY

The data that support the findings of this study are available from the corresponding author upon reasonable request.

APPENDIX: ENERGY SPECTRUM

The energy spectrum of the exciton–polariton system for a specific value of coherent pump intensity F was obtained numerically, integrating the time evolution of the photonic component given by Eq. (1). This procedure was repeated for the given value of polariton wave vector $\mathbf{k} = k_x$ and laser energy $E_p = \hbar\omega_p$. The dispersion from Fig. 6(a) was obtained realizing 51 200 simulations, performed using

the four-order Runge–Kutta method, for different values of (k_x, E_p) from the range $k_x \in (-6, 6) \mu\text{m}^{-1}$ and $E_p \in (-10, 30) \text{ meV}$. The time window of each simulation $(0, t_{\text{max}})$ was equal to $t_{\text{max}} = 80\tau_C$ and was enough to achieve a steady state of the system. Each simulation was obtained for 3200 algorithm iterations with a time step $dt = 0.025 \text{ ps}$. The analytical dispersion relations of exciton–polaritons, shown as the red lines, were obtained using the following formula:

$$E_{\text{UP,LP}} = \frac{1}{2} (E_X(\mathbf{k}) + E_C(\mathbf{k}) - i\hbar(\gamma_C + \gamma_X) \pm \sqrt{\hbar^2\Omega_R^2 + (\Delta - i\hbar(\gamma_C - \gamma_X))^2}) + \Delta_B, \quad (\text{A1})$$

where $\Delta = E_C(\mathbf{k}) - E_X(\mathbf{k})$ is the detuning and Δ_B is the numerically calculated value of blueshift (see the details in the main text). The corresponding Hopfield coefficients for the upper polaritons are given by⁸⁰

$$|X_U(\mathbf{k})|^2 = 1 - \frac{1}{2} \left(1 - \frac{\Delta - \Delta_B}{\sqrt{(\Delta - \Delta_B)^2 + \hbar^2\Omega_R^2}} \right), \quad (\text{A2})$$

$$|C_U(\mathbf{k})|^2 = 1 - \frac{1}{2} \left(1 + \frac{\Delta - \Delta_B}{\sqrt{(\Delta - \Delta_B)^2 + \hbar^2\Omega_R^2}} \right). \quad (\text{A3})$$

REFERENCES

- ¹A. Kavokin, J. J. Baumberg, G. Malpuech, and F. P. Laussy, *Microcavities* (Oxford University Press, 2017).
- ²I. Carusotto and C. Ciuti, “Quantum fluids of light,” *Rev. Mod. Phys.* **85**, 299–366 (2013).
- ³A. Szöke, V. Daneu, J. Goldhar, and N. A. Kurnit, “Bistable optical element and its applications,” *Appl. Phys. Lett.* **15**, 376–379 (1969).
- ⁴H. Gibbs, *Optical Bistability: Controlling Light with Light* (Elsevier, 2012).
- ⁵H. M. Gibbs, S. L. McCall, and T. N. C. Venkatesan, “Differential gain and bistability using a sodium-filled Fabry–Perot interferometer,” *Phys. Rev. Lett.* **36**, 1135–1138 (1976).
- ⁶H. M. Gibbs, S. L. McCall, T. N. C. Venkatesan, A. C. Gossard, A. Passner, and W. Wiegmann, “Optical bistability in semiconductors,” *Appl. Phys. Lett.* **35**, 451–453 (1979).
- ⁷Z. Geng, K. J. H. Peters, A. A. P. Trichet, K. Malmir, R. Kolkowski, J. M. Smith, and S. R. K. Rodriguez, “Universal scaling in the dynamic hysteresis, and non-Markovian dynamics, of a tunable optical cavity,” *Phys. Rev. Lett.* **124**, 153603 (2020).
- ⁸A. Joshi, A. Brown, H. Wang, and M. Xiao, “Controlling optical bistability in a three-level atomic system,” *Phys. Rev. A* **67**, 041801 (2003).
- ⁹S. Gupta, K. L. Moore, K. W. Murch, and D. M. Stamper-Kurn, “Cavity nonlinear optics at low photon numbers from collective atomic motion,” *Phys. Rev. Lett.* **99**, 213601 (2007).
- ¹⁰H. Gothe, T. Valenzuela, M. Cristiani, and J. Eschner, “Optical bistability and nonlinear dynamics by saturation of cold Yb atoms in a cavity,” *Phys. Rev. A* **99**, 013849 (2019).
- ¹¹N. K. Dutta, G. P. Agrawal, and M. W. Focht, “Bistability in coupled cavity semiconductor lasers,” *Appl. Phys. Lett.* **44**, 30–32 (1984).
- ¹²R. Roy and L. Mandel, “Optical bistability and first order phase transition in a ring dye laser,” *Opt. Commun.* **34**, 133–136 (1980).
- ¹³P. Jung, G. Gray, R. Roy, and P. Mandel, “Scaling law for dynamical hysteresis,” *Phys. Rev. Lett.* **65**, 1873–1876 (1990).
- ¹⁴M. Soljačić, M. Ibanescu, C. Luo, S. G. Johnson, S. Fan, Y. Fink, and J. D. Joannopoulos, “All-optical switching using optical bistability in nonlinear photonic crystals,” in *Photonic Crystal Materials and Devices* (SPIE, 2003), Vol. 5000, pp. 200–214.
- ¹⁵A. Majumdar and A. Rundquist, “Cavity-enabled self-electro-optic bistability in silicon photonics,” *Opt. Lett.* **39**, 3864–3867 (2014).
- ¹⁶H. Kawaguchi, “Bistable laser diodes and their applications: State of the art,” *IEEE J. Sel. Top. Quantum Electron.* **3**, 1254–1270 (1997).
- ¹⁷C. F. Marki, D. R. Jorgesen, H. Zhang, P. Wen, and S. C. Esener, “Observation of counterclockwise, clockwise and butterfly bistability in 1550 nm VCSOs,” *Opt. Express* **15**, 4953–4959 (2007).
- ¹⁸A. Hurtado, A. Quirce, A. Valle, L. Pesquera, and M. J. Adams, “Power and wavelength polarization bistability with very wide hysteresis cycles in a 1550 nm-VCSEL subject to orthogonal optical injection,” *Opt. Express* **17**, 23637–23642 (2009).
- ¹⁹H. Xie, S. Jiang, J. Shan, and K. F. Mak, “Valley-selective exciton bistability in a suspended monolayer semiconductor,” *Nano Lett.* **18**, 3213–3220 (2018).
- ²⁰C. Min, P. Wang, C. Chen, Y. Deng, Y. Lu, H. Ming, T. Ning, Y. Zhou, and G. Yang, “All-optical switching in subwavelength metallic grating structure containing nonlinear optical materials,” *Opt. Lett.* **33**, 869–871 (2008).
- ²¹A. Tredicucci, Y. Chen, V. Pellegrini, M. Börger, and F. Bassani, “Optical bistability of semiconductor microcavities in the strong-coupling regime,” *Phys. Rev. A* **54**, 3493–3498 (1996).
- ²²A. Baas, J. P. Karr, H. Eleuch, and E. Giacobino, “Optical bistability in semiconductor microcavities,” *Phys. Rev. A* **69**, 023809 (2004).
- ²³F. Claude, M. J. Jacquet, R. Usciat, I. Carusotto, E. Giacobino, A. Bramati, and Q. Glorieux, “High-resolution coherent probe spectroscopy of a polariton quantum fluid,” *Phys. Rev. Lett.* **129**, 103601 (2022).
- ²⁴N. A. Gippius, S. G. Tikhodeev, V. D. Kulakovskii, D. N. Krizhanovskii, and A. I. Tartakovskii, “Nonlinear dynamics of polariton scattering in semiconductor microcavity: Bistability vs stimulated scattering,” *Europhys. Lett.* **67**, 997 (2004).
- ²⁵E. A. Cotta and F. M. Matinaga, “Bistability double-crossing curve effect in a polariton-laser semiconductor microcavity,” *Phys. Rev. B* **76**, 073308 (2007).
- ²⁶N. A. Gippius, I. A. Shelykh, D. D. Solnyshkov, S. S. Gavrilov, Y. G. Rubo, A. V. Kavokin, S. G. Tikhodeev, and G. Malpuech, “Polarization multistability of cavity polaritons,” *Phys. Rev. Lett.* **98**, 236401 (2007).
- ²⁷T. K. Paraíso, M. Wouters, Y. Léger, F. Morier-Genoud, and B. Deveaud-Plédran, “Multistability of a coherent spin ensemble in a semiconductor microcavity,” *Nat. Mater.* **9**, 655–660 (2010).
- ²⁸L. Pickup, K. Kalinin, A. Askitopoulos, Z. Hatzopoulos, P. G. Savvidis, N. G. Berloff, and P. G. Lagoudakis, “Optical bistability under nonresonant excitation in spinor polariton condensates,” *Phys. Rev. Lett.* **120**, 225301 (2018).
- ²⁹Y. del Valle-Inclán Redondo, H. Sigurdsson, H. Ohadi, I. A. Shelykh, Y. G. Rubo, Z. Hatzopoulos, P. G. Savvidis, and J. J. Baumberg, “Observation of inversion, hysteresis, and collapse of spin in optically trapped polariton condensates,” *Phys. Rev. B* **99**, 165311 (2019).
- ³⁰H. Sigurdsson, “Hysteresis in linearly polarized nonresonantly driven exciton–polariton condensates,” *Phys. Rev. Res.* **2**, 023323 (2020).
- ³¹T. C. H. Liew, A. V. Kavokin, and I. A. Shelykh, “Optical circuits based on polariton neurons in semiconductor microcavities,” *Phys. Rev. Lett.* **101**, 016402 (2008).
- ³²T. C. H. Liew, A. V. Kavokin, T. Ostatnický, M. Kaliteevski, I. A. Shelykh, and R. A. Abram, “Exciton–polariton integrated circuits,” *Phys. Rev. B* **82**, 033302 (2010).
- ³³M. Foss-Feig, P. Niroula, J. T. Young, M. Hafezi, A. V. Gorshkov, R. M. Wilson, and M. F. Maghrebi, “Emergent equilibrium in many-body optical bistability,” *Phys. Rev. A* **95**, 043826 (2017).
- ³⁴O. Kyriienko, H. Sigurdsson, and T. C. H. Liew, “Probabilistic solving of NP-hard problems with bistable nonlinear optical networks,” *Phys. Rev. B* **99**, 195301 (2019).
- ³⁵I. A. Shelykh, T. C. H. Liew, and A. V. Kavokin, “Spin rings in semiconductor microcavities,” *Phys. Rev. Lett.* **100**, 116401 (2008).
- ³⁶H. Suchomel, S. Brodbeck, T. C. H. Liew, M. Amthor, M. Klaas, S. Klemmt, M. Kamp, S. Höfling, and C. Schneider, “Prototype of a bistable polariton field-effect transistor switch,” *Sci. Rep.* **7**, 5114 (2017).

- ³⁷D. Ballarini, M. De Giorgi, E. Cancellieri, R. Houdré, E. Giacobino, R. Cin-
golani, A. Bramati, G. Gigli, and D. Sanvitto, "All-optical polariton transistor," *Nat. Commun.* **4**, 1778 (2013).
- ³⁸T. Espinosa-Ortega and T. C. H. Liew, "Complete architecture of integrated
photonic circuits based on AND and NOT logic gates of exciton polaritons in
semiconductor microcavities," *Phys. Rev. B* **87**, 195305 (2013).
- ³⁹A. Baas, J.-P. Karr, M. Romanelli, A. Bramati, and E. Giacobino, "Optical bista-
bility in semiconductor microcavities in the nondegenerate parametric oscillation
regime: Analogy with the optical parametric oscillator," *Phys. Rev. B* **70**, 161307
(2004).
- ⁴⁰L. W. Tutt and T. F. Boggess, "A review of optical limiting mechanisms and
devices using organics, fullerenes, semiconductors and other materials," *Prog.*
Quantum Electron. **17**, 299–338 (1993).
- ⁴¹R. Gadhwal and A. Devi, "A review on the development of optical limiters from
homogeneous to reflective 1-D photonic crystal structures," *Opt. Laser Technol.*
141, 107144 (2021).
- ⁴²R. Gadhwal, P. Kaushik, and A. Devi, "A review on 1D photonic crystal based
reflective optical limiters," *Crit. Rev. Solid State Mater. Sci.* **48**, 93–111 (2023).
- ⁴³J. H. Vella, J. H. Goldsmith, A. T. Browning, N. I. Limberopoulos, I. Vitebskiy,
E. Makri, and T. Kottos, "Experimental realization of a reflective optical limiter,"
Phys. Rev. Appl. **5**, 064010 (2016).
- ⁴⁴E. Makri, H. Ramezani, T. Kottos, and I. Vitebskiy, "Concept of a reflective
power limiter based on nonlinear localized modes," *Phys. Rev. A* **89**, 031802
(2014).
- ⁴⁵G. S. He, L.-S. Tan, Q. Zheng, and P. N. Prasad, "Multiphoton absorbing materi-
als: Molecular designs, characterizations, and applications," *Chem. Rev.* **108**,
1245–1330 (2008).
- ⁴⁶J. W. Perry, K. Mansour, I.-Y. S. Lee, X.-L. Wu, P. V. Bedworth, C.-T. Chen,
D. Ng, S. R. Marder, P. Miles, T. Wada, M. Tian, and H. Sasabe, "Organic opti-
cal limiter with a strong nonlinear absorptive response," *Science* **273**, 1533–1536
(1996).
- ⁴⁷D. Dini, M. J. F. Calvete, and M. Hanack, "Nonlinear optical materials for the
smart filtering of optical radiation," *Chem. Rev.* **116**, 13043–13233 (2016).
- ⁴⁸R. C. C. Leite, S. P. S. Porto, and T. C. Damen, "The thermal lens effect as a
power-limiting device," *Appl. Phys. Lett.* **10**, 100–101 (1967).
- ⁴⁹L. Vivien, P. Lançon, D. Riehl, F. Hache, and E. Anglaret, "Carbon nanotubes
for optical limiting," *Carbon* **40**, 1789–1797 (2002).
- ⁵⁰D. J. Hagan, "Optical limiting," in *Handbook of Optics, Third Edition Volume*
IV: Optical Properties of Materials, Nonlinear Optics, Quantum Optics (Set), 3rd
ed., edited by M. Bass, C. Decusatis, J. M. Enoch, V. Lakshminarayanan, G. Li,
C. MacDonald, V. N. Mahajan, and E. Van Stryland (McGraw-Hill Education,
2009), Chap. 13.
- ⁵¹S. Husaini, H. Teng, and V. M. Menon, "Enhanced nonlinear optical response
of metal nanocomposite based photonic crystals," *Appl. Phys. Lett.* **101**, 111103
(2012).
- ⁵²S. Yan, J. Dong, A. Zheng, and X. Zhang, "Chip-integrated optical power limiter
based on an all-passive micro-ring resonator," *Sci. Rep.* **4**, 6676 (2014).
- ⁵³M. Heinrich, F. Eilenberger, R. Keil, F. Dreisow, E. Suran, F. Louradour,
A. Tünnermann, T. Pertsch, S. Nolte, and A. Szameit, "Optical limiting and spec-
tral stabilization in segmented photonic lattices," *Opt. Express* **20**, 27299–27310
(2012).
- ⁵⁴U. Kuhl, F. Mortessagne, E. Makri, I. Vitebskiy, and T. Kottos, "Waveguide pho-
tonic limiters based on topologically protected resonant modes," *Phys. Rev. B* **95**,
121409 (2017).
- ⁵⁵A. A. Ryzhov, "Optical limiting performance of a GaAs/AlAs heterostructure
microcavity in the near-infrared," *Appl. Opt.* **56**, 5811 (2017).
- ⁵⁶D. Sanvitto and S. Kéna-Cohen, "The road towards polaritonic devices," *Nat.*
Mater. **15**, 1061–1073 (2016).
- ⁵⁷H. Ulmer-Tuffigo, F. Kany, G. Feuillet, R. Langer, J. Bleuse, and J. L. Pautrat,
"Magnetic tuning of resonance in semimagnetic semiconductor microcavities,"
J. Cryst. Growth **159**, 605–608 (1996).
- ⁵⁸M. Richard, J. Kasprzak, R. André, R. Romestain, L. S. Dang, G. Malpuech,
and A. Kavokin, "Experimental evidence for nonequilibrium Bose condensation
of exciton polaritons," *Phys. Rev. B* **72**, 201301 (2005).
- ⁵⁹D. P. Cubian, M. Haddad, R. André, R. Frey, G. Roosen, J. L. A. Diego,
and C. Flytzanis, "Photoinduced magneto-optic Kerr effects in asymmetric
semiconductor microcavities," *Phys. Rev. B* **67**, 045308 (2003).
- ⁶⁰J.-G. Rousset, B. Piętko, M. Król, R. Mirek, K. Lekenta, J. Szczytko, J. Borysiuk,
J. Suffczynski, T. Kazimierzczuk, M. Goryca, T. Smoleński, P. Kossacki, M.
Nawrocki, and W. Pacuski, "Strong coupling and polariton lasing in Te based
microcavities embedding (Cd, Zn)Te quantum wells," *Appl. Phys. Lett.* **107**,
201109 (2015).
- ⁶¹D. Scalbert, M. Vladimirova, A. Brunetti, S. Cronenberger, M. Nawrocki,
J. Bloch, A. V. Kavokin, I. A. Shelykh, R. André, D. Solnyshkov, and G. Malpuech,
"Polariton spin beats in semiconductor quantum well microcavities," *Superlattices*
Microstruct. **43**, 417–426 (2008).
- ⁶²C. Gourdon, G. Lazard, V. Jeudy, C. Testelin, E. L. Ivchenko, and G. Karczewski,
"Enhanced Faraday rotation in CdMnTe quantum wells embedded in an optical
cavity," *Solid State Commun.* **123**, 299–304 (2002).
- ⁶³S. Bieker, P. R. Hartmann, T. Kießling, M. Rüh, C. Schumacher, C. Gould,
W. Ossau, and L. W. Molenkamp, "Removal of GaAs growth substrates from
II–VI semiconductor heterostructures," *Semicond. Sci. Technol.* **29**, 045016
(2014).
- ⁶⁴B. Seredyński, P. Starzyk, and W. Pacuski, "Exfoliation of epilayers with
quantum dots," *Mater. Today: Proc.* **4**, 7053–7058 (2017).
- ⁶⁵B. Seredyński, M. Król, P. Starzyk, R. Mirek, M. Ściesiek, K. Sobczak, J. Borysiuk,
D. Stephan, J.-G. Rousset, J. Szczytko, B. Piętko, and W. Pacuski, "(Cd, Zn, Mg)Te-
based microcavity on MgTe sacrificial buffer: Growth, lift-off, and transmission
studies of polaritons," *Phys. Rev. Mater.* **2**, 043406 (2018).
- ⁶⁶L. Dominici, M. Petrov, M. Matuszewski, D. Ballarini, M. De Giorgi, D. Colas,
E. Cancellieri, B. Silva Fernández, A. Bramati, G. Gigli, A. Kavokin, F. Laussy, and
D. Sanvitto, "Real-space collapse of a polariton condensate," *Nat. Commun.* **6**,
8993 (2015).
- ⁶⁷I. Y. Chestnov, T. A. Khudaiberganov, A. P. Alodjants, and A. V. Kavokin,
"Heat-assisted self-localization of exciton polaritons," *Phys. Rev. B* **98**, 115302
(2018).
- ⁶⁸D. Ballarini, I. Chestnov, D. Caputo, M. De Giorgi, L. Dominici, K. West, L. N.
Pfeiffer, G. Gigli, A. Kavokin, and D. Sanvitto, "Self-trapping of exciton–polariton
condensates in GaAs microcavities," *Phys. Rev. Lett.* **123**, 047401 (2019).
- ⁶⁹C. Ciuti, P. Schwendimann, and A. Quattropani, "Theory of polariton para-
metric interactions in semiconductor microcavities," *Semicond. Sci. Technol.* **18**,
S279–S293 (2003).
- ⁷⁰I. Carusotto and C. Ciuti, "Probing microcavity polariton superfluidity through
resonant Rayleigh scattering," *Phys. Rev. Lett.* **93**, 166401 (2004).
- ⁷¹N. S. Voronova, A. A. Elistratov, and Y. E. Lozovik, "Detuning-controlled inter-
nal oscillations in an exciton–polariton condensate," *Phys. Rev. Lett.* **115**, 186402
(2015).
- ⁷²A. Rahmani, D. Colas, N. Voronova, K. Jamshidi-Ghaleh, L. Dominici, and
F. P. Laussy, "Topologically driven Rabi-oscillating interference dislocation,"
Nanophotonics **11**, 2909–2919 (2022).
- ⁷³A. Rahmani and L. Dominici, "Detuning control of Rabi vortex oscillations in
light–matter coupling," *Phys. Rev. B* **100**, 094310 (2019).
- ⁷⁴L. Dominici, D. Colas, A. Gianfrate, A. Rahmani, V. Ardizzone, D. Ballarini,
M. De Giorgi, G. Gigli, F. P. Laussy, D. Sanvitto, and N. Voronova, "Full-Bloch
beams and ultrafast Rabi-rotating vortices," *Phys. Rev. Res.* **3**, 013007 (2021).
- ⁷⁵A. Zamora, G. Dagvadorj, P. Comaron, I. Carusotto, N. P. Proukakis, and
M. H. Szymańska, "Kibble–Zurek mechanism in driven dissipative systems
crossing a nonequilibrium phase transition," *Phys. Rev. Lett.* **125**, 095301 (2020).
- ⁷⁶D. Sanvitto, F. M. Marchetti, M. H. Szymańska, G. Tosi, M. Baudisch, F. P.
Laussy, D. N. Krizhanovskii, M. S. Skolnick, L. Marrucci, A. Lemaître, J. Bloch,
C. Tejedor, and L. Viña, "Persistent currents and quantized vortices in a polariton
superfluid," *Nat. Phys.* **6**, 527–533 (2010).
- ⁷⁷I. Iorsh, A. Alodjants, and I. A. Shelykh, "Microcavity with saturable nonlin-
earity under simultaneous resonant and nonresonant pumping: Multistability,

Hopf bifurcations and chaotic behaviour,” *Opt. Express* **24**, 11505–11514 (2016).

⁷⁸E. Cancellieri, F. M. Marchetti, M. H. Szymańska, and C. Tejedor, “Multistability of a two-component exciton–polariton fluid,” *Phys. Rev. B* **83**, 214507 (2011).

⁷⁹C. Lange, E. Cancellieri, D. Panna, D. M. Whittaker, M. Steger, D. W. Snoke, L. N. Pfeiffer, K. W. West, and A. Hayat, “Ultrafast control of strong light–matter coupling,” *New J. Phys.* **20**, 013032 (2018).

⁸⁰H. Deng, H. Haug, and Y. Yamamoto, “Exciton–polariton Bose–Einstein condensation,” *Rev. Mod. Phys.* **82**, 1489–1537 (2010).